IgA-Fcα/μR-induced neutrophil extracellular traps formation in intestinal mucosal injury in murine IgA vasculitis

FENG-XIA QIN[1*], YU-LAN LIN[1*], QING TANG[1], LI HUANG[1], LIAN-CHENG LAN[1], XIANG YUN[1] and XIU-QI CHEN[1,2]

[1]Children's Health Center, The First Affiliated Hospital, Guangxi Medical University, Nanning, Guangxi Zhuang Autonomous Region 530021, P.R. China; [2]Difficult and Critical Illness Center, Pediatric Clinical Medical Research Center of Guangxi, Nanning, Guangxi Zhuang Autonomous Region 530021, P.R. China

Received February 2, 2026; Accepted October 9, 2026

DOI: 10.3892/etm.2026.13359

Abstract. IgA vasculitis (IgAV) is a common systemic vasculitis in which IgA immune complexes activate neutrophils via Fc receptors to produce neutrophil extracellular traps (NETs). However, mice lack human FcαRI and instead express Fcα/μR. The present study aimed to investigate the role of Fcα/μR in NET formation in a murine model of IgAV and to elucidate the potential mechanism by which NETs contribute to intestinal mucosal microvascular endothelial cell injury. A total of 12 Fcamr-knockout (Fcamr-KO) mice and 12 wild-type (WT) mice were randomly assigned to four groups: WT model, WT control, Fcamr-KO model and Fcamr-KO control groups. The IgAV model was established through sequential injections of India ink and an emulsified mixture of Freund's complete adjuvant and ovalbumin, followed by an ovalbumin challenge. IgA and complement C3 deposition in renal and intestinal tissues was evaluated using immunofluorescence staining. Plasma cell-free DNA levels were quantified using the Quant-iT PicoGreen assay. The concentrations of NET components (MPO-DNA and NE-DNA) and inflammatory cytokines (IL-1β and IL-18) in intestinal tissue homogenates were measured using enzyme-linked immunosorbent assays. The protein expression levels of NOD-like receptor pyrin domain-containing protein 3 (NLRP3), ASC, cleaved caspase-1 and the N-terminal fragment of GSDMD (GSDMD-N) were determined by western blotting. Intestinal histopathological changes were evaluated by hematoxylin and eosin staining, and cellular ultrastructure was examined using transmission electron microscopy (TEM). Compared with the WT control group, the WT model group exhibited significantly greater IgA and C3 deposition, elevated levels of NET markers (MPO-DNA and NE-DNA) and increased expression of pyroptosis-related cytokines (IL-1β and IL-18) and key proteins in the NLRP3 inflammasome pathway (NLRP3, ASC, cleaved caspase-1 and GSDMD-N). TEM revealed characteristic pyroptotic morphological changes in intestinal mucosal microvascular endothelial cells in the WT model group. By contrast, all of these pathological alterations were markedly attenuated in the Fcamr-KO model group. Notably, NET levels and pyroptosis pathway activation in Fcamr-KO model mice were comparable to those observed in both the WT and Fcamr-KO control groups. These findings indicate that IgA promotes NET formation in an Fcα/μR-dependent manner. Furthermore, NETs may induce pyroptosis in intestinal mucosal microvascular endothelial cells by activating the NLRP3-ASC-caspase-1 inflammasome axis, thereby contributing to the pathogenesis of intestinal mucosal injury in IgAV.

Introduction

IgA vasculitis (IgAV), formerly known as Henoch-Schönlein purpura, is the most common systemic vasculitis in children. Its characteristic clinical manifestations include palpable purpura, arthralgia or arthritis, abdominal pain and renal involvement (1-3). IgAV occurs more frequently in autumn and winter and predominantly affects children aged 3-15 years, with an estimated annual incidence of ~1 in 6,660 to 1 in 4,880 children (4). Although the clinical manifestations of IgAV have been well characterized, its underlying pathogenesis, particularly the molecular mechanisms responsible for severe intestinal complications, remains incompletely understood.

Current evidence suggests that IgAV pathogenesis is closely associated with the deposition of immune complexes, particularly those containing aberrantly glycosylated IgA1, complement activation, inflammatory mediator release and genetic susceptibility (5-7). Studies have further suggested that immune complexes containing aberrantly glycosylated IgA1 activate neutrophils and induce the formation of

Correspondence to: Professor Xiu-Qi Chen or Professor Xiang Yun, Children's Health Center, The First Affiliated Hospital, Guangxi Medical University, 6 Shuangyong Road, Nanning, Guangxi Zhuang Autonomous Region 530021, P.R. China
E-mail: chenxiuqi@gxmu.edu.cn
E-mail: bnfeiyun@aliyun.com

*Contributed equally

Key words: IgA vasculitis, Fcα/μ receptor, neutrophil extracellular traps, pyroptosis, NOD-like receptor pyrin domain-containing protein 3 inflammasome

neutrophil extracellular traps (NETs), thereby contributing to vascular inflammation (6,8-10). NETs are web-like structures consisting of decondensed chromatin decorated with antimicrobial proteins, including histones, myeloperoxidase (MPO) and neutrophil elastase (NE). Although NETs play a notable role in innate host defense by trapping pathogens, their excessive or dysregulated formation can cause tissue injury and promote autoimmune responses (11-13). Our previous research demonstrated that NET levels were notably elevated in the peripheral blood and affected tissues of children with IgAV and were correlated with disease severity (14). Moreover, enzymatic degradation of NETs using DNase I attenuated tissue injury in a rat model of IgAV (15). Collectively, these findings suggest that NETs may represent a key mechanistic link between immune complex deposition and end-organ injury. Nevertheless, whether NETs directly contribute to intestinal mucosal microvascular endothelial cell injury in IgAV and the precise molecular pathways involved remain unclear.

Pyroptosis is a form of programmed cell death mediated by caspases 1, 4, 5 and 11 and is characterized by plasma membrane pore formation, cellular swelling and the release of proinflammatory cytokines, including interleukin-1 beta (IL-1β) and IL-18 (16-18). A central regulator of this process is the NOD-like receptor pyrin domain-containing protein 3 (NLRP3) inflammasome, an intracellular multiprotein complex that functions as a pattern-recognition platform. The NLRP3 inflammasome can be activated by diverse pathogen-associated molecular patterns and damage-associated molecular patterns (DAMPs), resulting in the recruitment of the adaptor protein ASC and subsequent activation of caspase-1. Activated caspase-1 cleaves gasdermin D (GSDMD) to generate its N-terminal fragment (GSDMD-N), which forms pores in the plasma membrane and induces pyroptosis (19,20). Growing evidence implicates pyroptosis in the pathogenesis of various vascular inflammatory diseases (21-25). Notably, NETs and their components, including histones, have been identified as potent DAMPs capable of activating the NLRP3 inflammasome (13,26-28).

IgA immune complexes generally exert their immunostimulatory effects by engaging Fc receptors expressed on immune cells. In humans, FcαRI (CD89) is the principal Fc receptor for IgA (29); however, mice lack a direct ortholog of human FcαRI. Instead, mice express Fcα/μR (CD351), a receptor that binds both IgA and IgM and may functionally compensate for the absence of FcαRI by mediating the recognition of and signaling by IgA-containing immune complexes (30,31). Whether Fcα/μR contributes to NET formation in murine IgAV has not yet been investigated. Therefore, the present study used wild-type (WT) and Fcα/μR-knockout (Fcamr-KO) mice in a murine model of IgAV to investigate the role of Fcα/μR in NET-mediated tissue injury and elucidate the underlying molecular mechanisms.

Materials and methods

Experimental animals grouping and blinding. A total of 24 specific pathogen-free (SPF) mice were included in this study, comprising 12 C57BL/6J WT mice and 12 Fcamr-KO mice, all aged 3-5 weeks and weighing 12-20 g. The WT mice were obtained from the Experimental Animal Center of Guangxi Medical University [Nanning, China; license No. SCXK (Gui) 2025-0005]. The Fcamr-KO mice were generated with technical support from Shanghai Model Organisms Center by CRISPR/Cas9-mediated deletion of exon 2 of the *Fcamr* gene, resulting in a 420-bp deletion in the knockout allele and consequent loss of gene function. All Fcamr-KO mice used in the present study were confirmed to be homozygous for the knockout allele by PCR genotyping using a Tissue DNA Extraction Kit (cat. no. NMS0001-50; Shanghai Model Organisms Center, Inc.) and 2X Phanta Flash Master Mix (cat. no. P510; Vazyme Biotech Co., Ltd.). To confirm the Fcamr knockout, genomic DNA was extracted from mouse tail tips and subjected to PCR genotyping using three primers in a single reaction: Forward primer P1 (5'-AATGCTGTACCC CCGACAAG-3') and reverse primers P2 (5'-AAAGGAGCG GACACTAAGCC-3') and P4 (5'-GGTAGCTCTACCCGA AAGGC-3'). The PCR conditions were as follows: Initial denaturation at 98˚C for 3 min; 32 cycles of 98˚C for 10 sec, 63˚C for 10 sec and 72˚C for 1 min; and a final extension at 72˚C for 5 min. In the wild-type allele, P1 and P2 amplify a 302-bp product. In the knockout allele, the 420-bp deletion removes the P2 binding site, allowing P1 and P4 to amplify a 429-bp product across the deletion junction. Heterozygous mice displayed both bands, whereas homozygous knockout mice displayed only the 429-bp band. PCR products were resolved on a 1% agarose gel and visualized under UV light. Genotyping results are shown in Fig. S1. All animals were housed under SPF conditions at the Experimental Animal Center of Guangxi Medical University.

The present study was designed as a randomized controlled animal experiment. Using a random-number table, the mice were randomly assigned to four groups (n=6 per group), with allocation concealed using sequentially numbered, opaque, sealed envelopes. The groups were as follows: i) WT model group, comprising WT mice subjected to IgAV induction; ii) WT control group, comprising WT mice without intervention; iii) Fcamr-KO model group, comprising Fcamr-KO mice subjected to IgAV induction; and iv) Fcamr-KO control group, comprising Fcamr-KO mice without intervention. The sample size was justified using the resource equation method (32), which ensured an error degree of freedom ≥10 for one-way analysis of variance. A group size of six mice complied with the reduction principle of the 3Rs and was consistent with previous rodent studies investigating NETs and pyroptosis (27,33-35). Before analysis, an independent researcher replaced all group labels with randomly generated codes. Blinding was maintained during immunofluorescence quantification, histopathological scoring and transmission electron microscopy (TEM) interpretation. The coding key was disclosed only after all data collection, and statistical analyses had been completed.

Model establishment and sample collection. The IgAV model was established using an immunization-based protocol. During the first 3 weeks, 75 μl of India ink (40 mg/kg) was injected via the tail vein to block the reticuloendothelial system. From weeks 4 to 9, the mice received weekly intraperitoneal injections of 0.2 ml of an emulsion prepared by mixing ovalbumin (OVA; 18 mg/kg; cat. no. HY-W250978; MedChemExpress) with an equal volume of Freund's complete adjuvant (cat.

no. HY-153808; MedChemExpress). In week 10, the mice received a final challenge consisting of intravenous injections of 50 μl of OVA (3 mg/ml) via the tail vein for three consecutive days.

Within 24 h after the final challenge, mice were monitored for predefined humane endpoints (>20% body weight loss, severe lethargy, intractable distress or extensive ulcerative lesions). No animals reached these humane endpoints or died unexpectedly during the study. Anesthesia was induced with 4% isoflurane and maintained at 2%. Adequate anesthetic depth was confirmed by the loss of righting reflex, pedal withdrawal reflex, tail pinch reflex and eyelid reflex. Blood samples (800-1,500 μl) were collected via retro-orbital bleeding. Immediately after blood collection, mice were euthanized by cervical dislocation, followed by bilateral thoracotomy to ensure death. Whole blood was divided into two aliquots: One was used for routine hematological analysis, and the other was centrifuged at 1,000 x g for 10 min at 4˚C to obtain plasma, which was stored at -80˚C. Kidney and intestinal tissues were harvested. One portion of each tissue was snap-frozen in liquid nitrogen and stored at -80˚C, whereas another portion was fixed in 4% paraformaldehyde at 4˚C overnight and embedded in paraffin at 60˚C. All samples were processed to avoid repeated freeze-thaw cycles.

Tissue immunofluorescence. Paraffin-embedded tissue sections were deparaffinized, rehydrated and subjected to antigen retrieval using EDTA buffer (cat. no. AFIHC057; Hunan Aifang Biotechnology Co., Ltd.). Endogenous peroxidase activity was quenched using 3% H_2O_2 (cat. no. AFIHC012; Hunan Aifang Biotechnology Co., Ltd.), followed by blocking with 3% bovine serum albumin (cat. no. AFIHC018; Hunan Aifang Biotechnology Co., Ltd.) at room temperature for 30 min. The sections were then incubated overnight at 4˚C with the following primary antibodies: rabbit anti-IgA (1:500; cat. no. PK38143; Abmart Pharmaceutical Technology Co., Ltd.) and mouse anti-C3 (1:500; cat. no. 66157-1-Ig; Proteintech Group, Inc.). After washing, the sections were incubated with the appropriate horseradish peroxidase (HRP)-conjugated secondary antibodies (ready-to-use; cat. no. AFIHC0014; Hunan Aifang Biotechnology Co., Ltd.) at room temperature for 1 h, and the signals were amplified using a tyramide signal amplification kit (cat. no. AFIHC033; Hunan Aifang Biotechnology Co., Ltd.). The nuclei were counterstained with DAPI (cat. no. AFIHC044, Hunan Aifang Biotechnology Co., Ltd.), and the slides were mounted using an antifade mounting medium. Images were acquired at 200x or 400x magnification using a fluorescence microscope (cat. no. AFBI0; Hunan Aifang Biotechnology Co., Ltd.).

Detection of NET components. Circulating cell-free DNA (cfDNA) in plasma was quantified using the Quant-iT™ PicoGreen™ dsDNA Assay Kit (cat. no. P7581; Invitrogen; Thermo Fisher Scientific, Inc.). After the reagents were equilibrated to room temperature, a standard curve was established and the working solution was prepared. Standards and plasma samples were then added to a blank 96-well plate, and background fluorescence was measured. Subsequently, the working solution was added, and the plate was incubated in the dark for 5 min. Total fluorescence was then measured. After subtracting the background fluorescence, plasma cfDNA concentrations were calculated using the regression equation of the standard curve.

To evaluate NET formation in intestinal tissues, the levels of MPO-DNA and NE-DNA complexes in intestinal tissue homogenate supernatants were measured using commercial ELISA kits specific for MPO-DNA (cat. no. MM-1177M1; Jiangsu Meimian Biotechnology Co., Ltd.) and NE-DNA (cat. no. MM-47326M1; Jiangsu Meimian Biotechnology Co., Ltd.), respectively, in accordance with the manufacturers' instructions. To prepare the tissue homogenates, intestinal tissues were weighed and homogenized in ice-cold 0.01 M phosphate-buffered saline (PBS; pH 7.4) at a ratio of 1 mg of tissue to 9 μl of PBS using a tissue grinder at 4˚C. The homogenates were then centrifuged at 5,000 x g for 20 min at 4˚C, and the resulting supernatants were collected for subsequent assays.

Evaluation of pyroptosis pathway activation. The concentrations of the pyroptosis-related cytokines IL-1β and IL-18 in intestinal tissue homogenates were measured using commercial ELISA kits (cat. nos. MM-0181H1 and MM-0169M1; Jiangsu Meimian Biotechnology Co., Ltd.).

The expression levels of the pyroptosis-associated proteins NLRP3, ASC, cleaved caspase-1 and GSDMD-N were determined by western blotting. Total protein was extracted from mouse intestinal tissues using RIPA lysis buffer (cat. no. xblot-012; Suzhou X-BLOT LifeScience Ltd.) and quantified using a BCA Protein Assay Kit (cat. no. P0012S; Beyotime Biotechnology). Equal amounts of protein (30 μg per lane) were separated by 10% sodium dodecyl sulfate-polyacrylamide gel electrophoresis and transferred onto polyvinylidene difluoride membranes (cat. no. ISEQ00010; MilliporeSigma). After blocking with 5% skimmed milk (cat. no. P0216-300g; Beyotime Biotechnology) at room temperature for 1.5 h, the membranes were incubated overnight at 4˚C with the following primary antibodies: Anti-NLRP3 (1:600; cat. no. YM8024; Immunoway Biotechnology Company), anti-ASC (1:1,000; cat. no. 340097; Chengdu Zen-Bioscience Co., Ltd.), anti-caspase-1 (1:1,000; cat. no. YC0002; Immunoway Biotechnology Company), which detects both pro-caspase-1 and cleaved caspase-1, anti-GSDMD (1:1,000; cat. no. F1568; Selleck Chemicals) and anti-β-actin (1:8,000; cat. no. GB15003; Wuhan Servicebio Technology Co., Ltd.). The membranes were subsequently incubated with the corresponding HRP-conjugated goat anti-rabbit IgG secondary antibody (1:10,000; cat. no. GB23303; Wuhan Servicebio Technology Co., Ltd.) at room temperature for 1 h. Protein bands were visualized using an enhanced chemiluminescence system (cat. no. BL523; Biosharp Life Sciences), and densitometric analysis was performed using ImageJ software (version 1.53q; National Institutes of Health).

Histopathological and ultrastructural analyses. For histopathological evaluation, intestinal tissue sections (4 μm thick) were stained with hematoxylin for 5 min and eosin for 1 min at room temperature (H&E) and examined for inflammatory cell infiltration, hemorrhage and edema using an upright light microscope. Histopathological changes were assessed according to the extent of intestinal villous and mucosal necrosis, hyperplasia and inflammatory cell infiltration. All

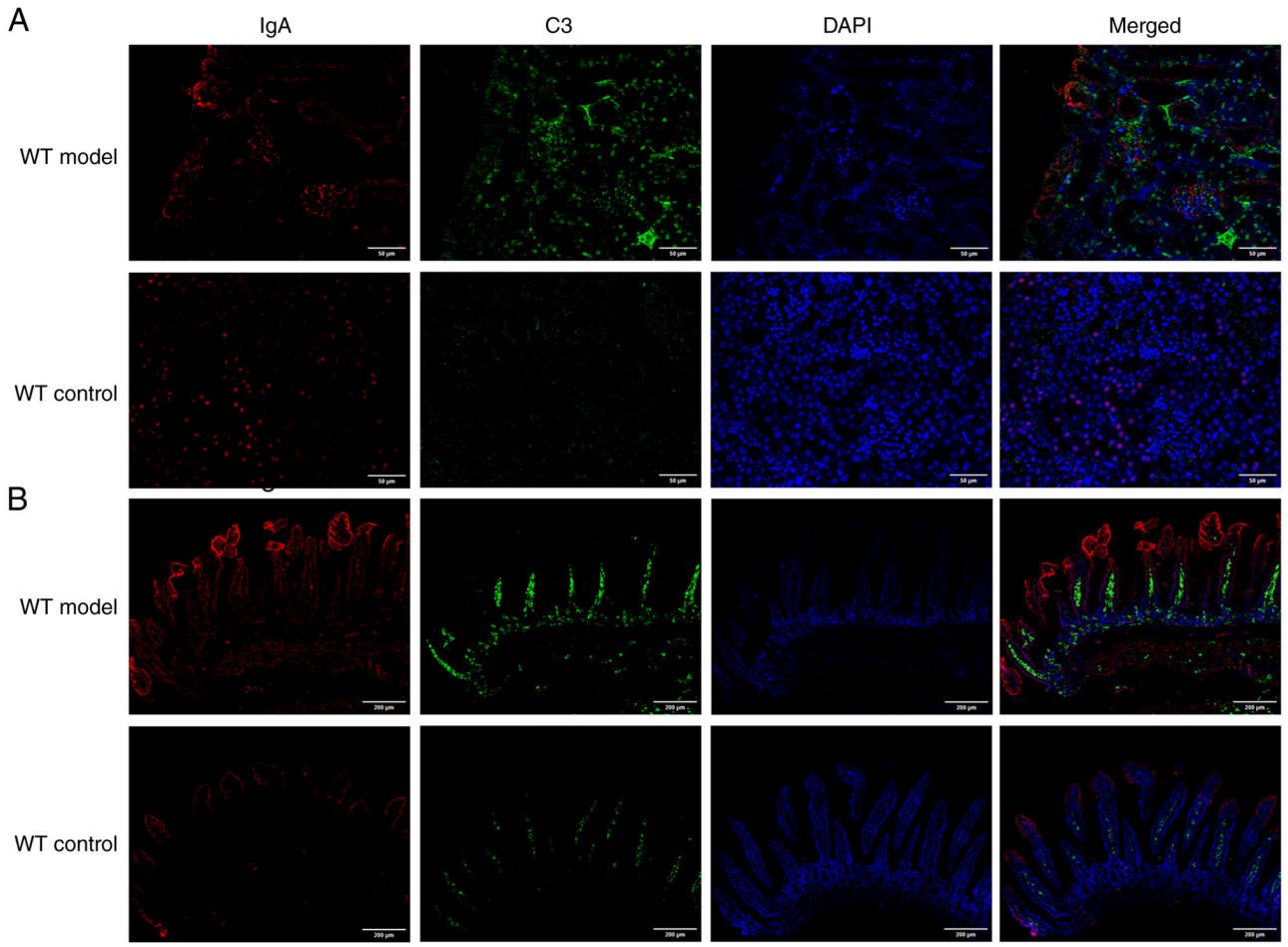


Figure 1. Representative immunofluorescence images showing IgA and C3 deposition. IgA and C3 deposition in (A) the kidney and (B) intestinal tissues of mice in the WT model and WT control groups. Data were obtained from 3 mice per group. Red signals indicate IgA, green signals indicate C3, and blue signals indicate DAPI. Merged images show the colocalization of IgA, C3 and DAPI signals. Scale bars, (A) 50 μm; (B) 200 μm. WT, wild-type.

sections were evaluated independently by two pathologists who were blinded to the group assignments, using a semi-quantitative five-point scale (0-4) adapted from the INHAND criteria (36): 0, normal; 1, minimal change; 2, mild change; 3, moderate change; and 4, marked or severe change.

For TEM, intestinal tissues were cut into 1-mm^3 pieces and fixed in 3% glutaraldehyde (cat. no. G1102; Wuhan Servicebio Technology Co., Ltd.) at 4˚C overnight. After dehydration, tissues were embedded in Epon-812 resin at 60˚C for 48 h. Ultrathin sections (80 nm) were prepared and double-stained with uranyl acetate for 10 min and lead citrate for 5 min at room temperature. Cellular ultrastructure, particularly that of microvascular endothelial cells, was examined using a TEM (JEM-1400FLASH; JOEL Ltd.) to assess membrane integrity, organelle morphology and characteristic features of pyroptosis, including cellular swelling and membrane pore formation.

Statistical analysis. Statistical analyses were performed using GraphPad Prism 9.0 (Dotmatics) and RStudio (version 2023.06.2+561; RStudio, Inc.). Data normality was assessed using the Shapiro-Wilk test, and homogeneity of variance was evaluated using Levene's test. For data with a two-factor design that met the assumptions of normality and homogeneity of variance, two-way analysis of variance was used; when a significant interaction was detected, simple effects analysis was performed with Bonferroni correction. For data that did not meet the assumptions of normality or homogeneity of variance, pairwise comparisons between groups were performed using Wilcoxon rank-sum tests, with P-values adjusted using the Bonferroni method. Sex was balanced across groups (3 males and 3 females per group). Given the small sample size (n=6 per group) and the study's focus on overall effects rather than sex differences, no sex-based subgroup analysis was performed. $P<0.05$ was considered to indicate a statistically significant difference.

Results

Successful establishment of the IgAV mouse model. Immunofluorescence staining revealed significantly greater deposition of IgA and complement C3 in both renal and intestinal tissues in the WT model group than in the WT control group (Fig. 1). These findings confirmed the successful establishment of the IgAV mouse model.

Fcα/μR may function as a key upstream receptor promoting NET formation in a mouse IgAV model. For plasma cfDNA, two-way ANOVA revealed a significant main effect of treatment ($F=26.400$; $P<0.001$), a significant main effect of genotype ($F=24.770$; $P<0.001$) and a significant interaction

Table I. Two-way ANOVA results for pyroptosis-related markers in intestinal tissues.

	Interaction		Treatment main effect		Genotype main effect	
Marker	F-value	P-value	F-value	P-value	F-value	P-value
IL-1β	8.388	0.0089	6.117	0.0225	26.42	<0.001
IL-18	24.940	<0.001	54.910	<0.001	22.170	<0.001
NLRP3	5.869	0.0250	19.260	<0.001	17.79	<0.001
ASC	21.440	<0.001	32.140	<0.001	15.950	<0.001
Cleaved caspase-1	13.880	0.0013	20.080	<0.001	8.708	0.0079
GSDMD-NT	14.560	0.0011	10.990	0.0035	8.077	0.0101

Data are presented as F- and P-values for the interaction, the main effect of treatment and the main effect of genotype. Two-way ANOVA was used with genotype and treatment as between-subject factors. GSDMD-NT, gasdermin D N-terminal; NLRP3, NOD-like receptor pyrin domain-containing protein 3; ASC, Apoptosis-associated speck-like protein containing a CARD.

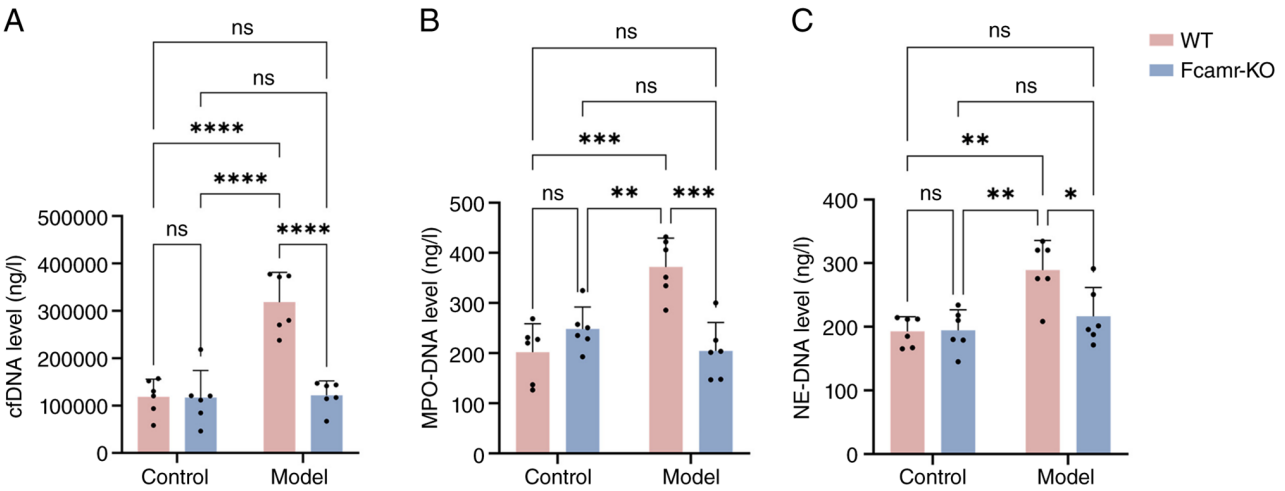


Figure 2. Levels of NET-related markers in the different experimental groups. (A) Plasma cfDNA levels. Levels of (B) MPO-DNA and (C) NE-DNA complexes in intestinal tissue homogenates, as quantified by ELISA. Data were obtained from six mice per group. Statistical significance was determined using two-way ANOVA to assess the main effects of genotype and treatment and their interaction. When a significant interaction was detected, simple effects analysis was performed with Bonferroni correction. *P<0.05, **P<0.01, ***P<0.001, ****P<0.0001; ns, not significant. cfNDA, cell free DNA; MPO, myeloperoxidase; NE, neutrophil elastase; WT, wild-type; Fcamr-KO, Fcα/μR-knockout.

(F=23.980; P<0.001). For intestinal MPO-DNA, two-way ANOVA revealed a significant main effect of treatment (F=8.162; P=0.0097), a significant main effect of genotype (F=7.551; P=0.0124) and a significant interaction (F=23.540; P<0.001). For intestinal NE-DNA, two-way ANOVA revealed a significant main effect of treatment (F=14.46; P=0.0011), a significant main effect of genotype (F=5.188; P=0.0339) and a significant interaction (F=5.746; P=0.0264).

Plasma cfDNA levels were significantly higher in the WT model group than in the WT control group (P<0.001; Fig. 2A). Similarly, intestinal tissue homogenates from WT model mice exhibited markedly elevated MPO-DNA and NE-DNA levels (P<0.001 and P=0.0017, respectively; Fig. 2B and C), indicating robust NET formation. By contrast, Fcamr-KO mice subjected to the same IgAV induction protocol showed no significant increases in cfDNA, MPO-DNA or NE-DNA levels, and these values were comparable to those observed in both the WT and Fcamr-KO control groups (all P>0.05; Fig. 2). Collectively, these findings indicate that Fcα/μR may act as a key upstream receptor that promotes NET formation in this murine model of IgAV.

Fcα/μR deficiency is associated with attenuated pyroptosis pathway activation in IgAV mice. To evaluate pyroptosis pathway activation, key molecular markers were measured. Two-way ANOVA revealed significant main effects of treatment and genotype, as well as significant interactions, for all measured pyroptosis-related markers (IL-1β, IL-18, NLRP3, ASC, cleaved caspase-1 and GSDMD-N; all P<0.05; Table I).

Simple effects analysis with Bonferroni correction showed that intestinal levels of the pyroptosis-associated cytokines IL-1β and IL-18 were significantly higher in the WT model group than in the WT control group (P=0.0068 and P<0.001, respectively; Fig. 3A and B). Consistently, western blot analysis revealed markedly increased intestinal expression of the pyroptosis executioner protein GSDMD-N and the core inflammasome components NLRP3, ASC and cleaved caspase-1 in WT model mice (all P<0.001; Fig. 3C-G). By

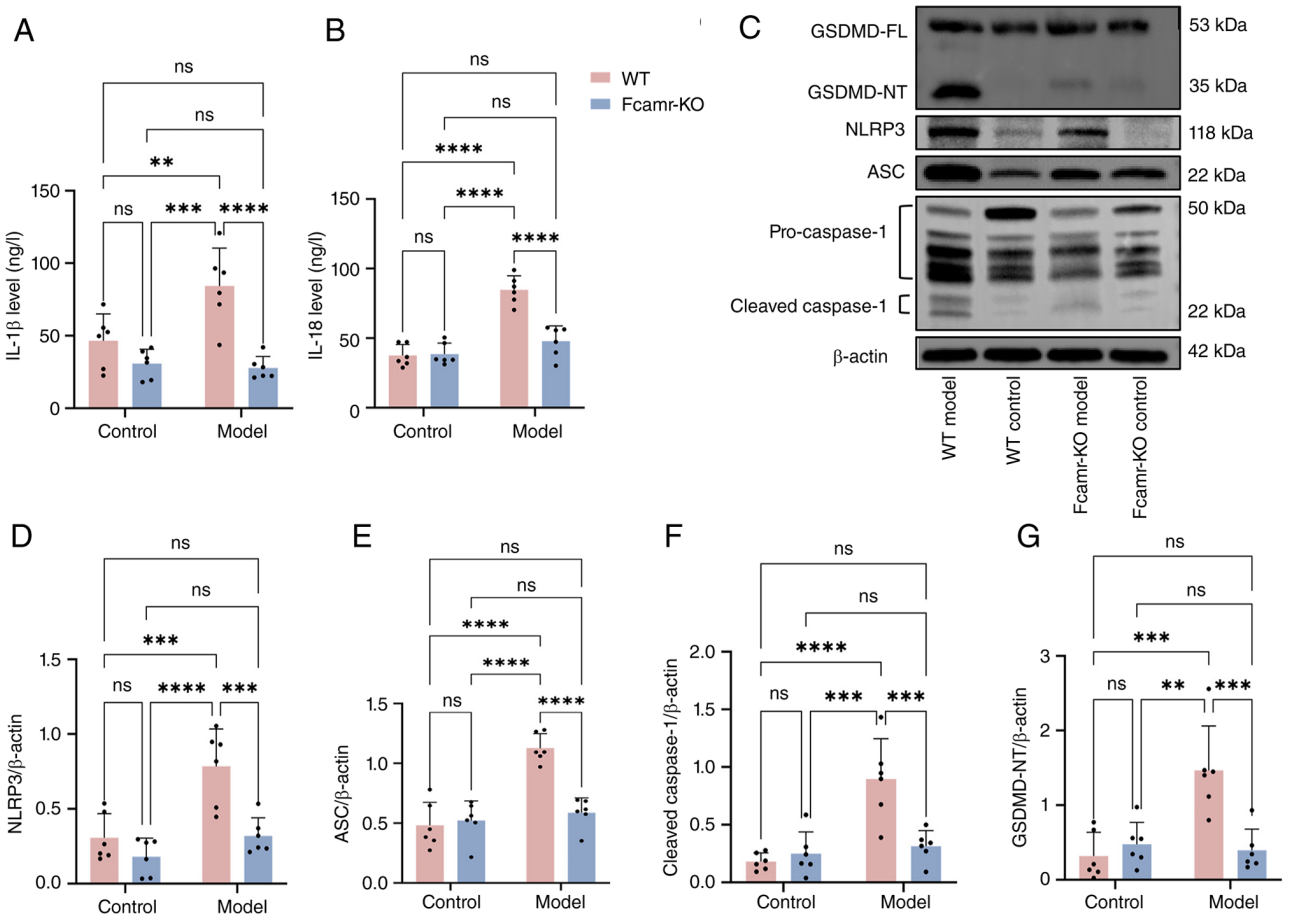


Figure 3. Analysis of pyroptosis-related molecules in intestinal tissues. Levels of the cytokines (A) IL-1β and (B) IL-18, as measured by ELISA. (C) Representative western blots and quantitative analyses of (D) NLRP3, (E) ASC, (F) cleaved caspase-1 and (G) GSDMD-N protein expression across the experimental groups. β-Actin was used as the loading control. Data were obtained from 6 biologically independent mice per group. Statistical significance was determined using two-way ANOVA to assess the main effects of genotype and treatment and their interaction. When a significant interaction was detected, simple effects analysis was performed with Bonferroni correction. **P<0.01, ***P<0.001, ****P<0.0001; ns, not significant. Fcamr-KO, Fcα/μR-knockout; GSDMD, gasdermin D; GSDMD-FL, GSDMD full length; GSDMD-NT, GSDMD N-terminal; NLRP3, NOD-like receptor pyrin domain-containing protein 3; ASC, Apoptosis-associated speck-like protein containing a CARD.

contrast, all molecular indicators of pyroptosis were significantly suppressed in the Fcamr-KO model group, with levels comparable to those in the WT and Fcamr-KO control groups (all P>0.05).

Fcα/μR deficiency attenuates pyroptosis in intestinal mucosal endothelial cells and alleviates barrier injury. TEM analysis revealed that, compared with the WT control group, intestinal microvascular endothelial cells in the WT model group exhibited characteristic ultrastructural features of pyroptosis, including plasma membrane rupture, mitochondrial swelling and disruption of intercellular junctions (Fig. 4A and B). Shortening and detachment of the microvilli were also observed, indicating marked intestinal mucosal barrier injury (Fig. 4C and D). By contrast, these morphological alterations were attenuated in the Fcamr-KO model group, in which no overt pyroptotic features were observed. The overall architecture of the intestinal mucosa and microvascular endothelial cells remained relatively intact in the Fcamr-KO model, Fcamr-KO control and WT control groups. Although minor structural alterations were observed in these groups, they were substantially less severe than those in the WT model group.

Fcα/μR deficiency ameliorates intestinal pathological injury. H&E staining revealed severe intestinal pathological changes in the WT model group, characterized by prominent inflammatory cell infiltration, tissue edema, hemorrhage and marked disruption of villous architecture (Fig. 4E and F). Semiquantitative scoring showed that the histopathological score was significantly higher in the WT model group than in the WT control group (P=0.025) and the Fcamr-KO control group (P=0.020), whereas the score was significantly lower in the Fcamr-KO model group than in the WT model group (P=0.026) (Fig. 4G).

Discussion

The present study suggests that Fcα/μR may function as a mediator of intestinal mucosal injury in a murine model of IgAV and provides preliminary evidence for its potential role in the upstream regulation of NET formation. In human IgAV, IgA-containing immune complexes are thought to activate neutrophils through FcαRI (CD89), potentially triggering NET release, a process implicated in vascular inflammation (6,10). Our previous clinical and experimental

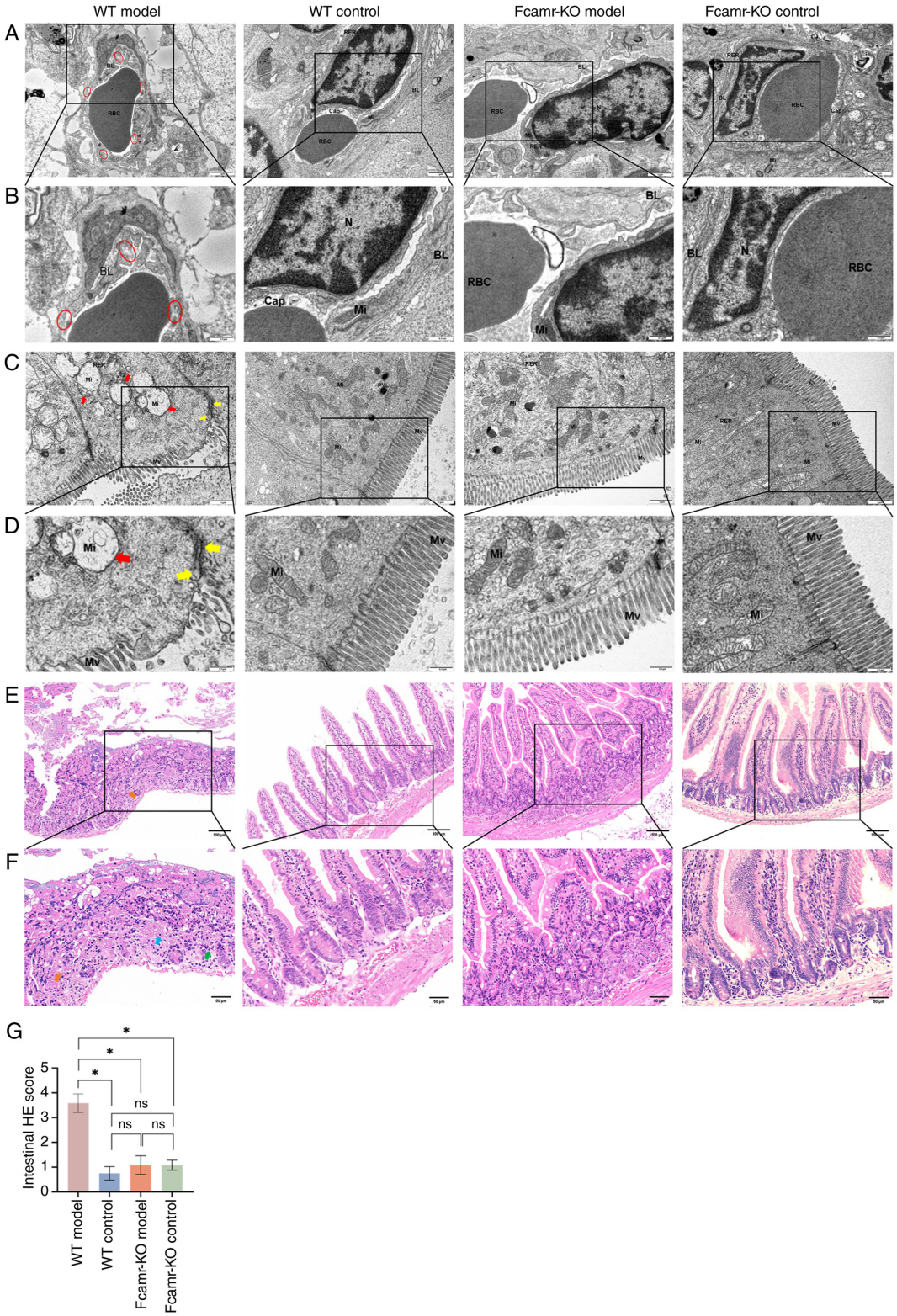


Figure 4. Assessment of intestinal mucosal injury in each experimental group using TEM and H&E staining. (A-D) Representative TEM images showing pyroptotic changes in intestinal microvascular endothelial cells and disruption of the intestinal mucosal barrier. Scale bars, (A and C) 1 μm; (B and D) 0.5 μm. Data were obtained from three biologically independent mice per group. (A) In the WT model group, TEM revealed blurred or discontinuous endothelial cell membranes (red circles), swollen mitochondria with indistinct cristae (red arrows) and disrupted intercellular junctions (yellow arrows). (B) Magnified inset of the boxed region in (A), showing detailed ultrastructural features of pyroptotic endothelial cells. (C) In the WT model group, TEM revealed shortened and effaced intestinal microvilli, markedly swollen mitochondria (red arrows) and disrupted intercellular junctions (yellow arrows). (D) Magnified inset of the boxed region in (C), showing detailed microvillous and mitochondrial alterations. (E and F) Representative H&E-stained images of intestinal mucosal tissues from each group. Data were obtained from 6 biologically independent mice per group. The WT model group exhibited necrotic, lysed and structurally indistinct intestinal villi, together with degeneration and necrosis of the mucosal layers (orange arrows). Marked inflammatory cell infiltration was observed, predominantly comprising polymorphonuclear neutrophils (green arrows) and lymphocytes (blue arrows). Scale bars, (E) 100 μm; (F) 50 μm. (G) Quantitative analysis of composite histopathological scores for intestinal tissue injury. Pairwise comparisons between groups were performed using Wilcoxon rank-sum tests, and P-values were adjusted using the Bonferroni method. *P<0.05; ns, not significant. Fcamr-KO, Fcα/μR-knockout; TEM, transmission electron microscopy; N, nucleus; Mi, mitochondrion; RER, rough endoplasmic reticulum; BL, basal lamina; Cap, capillary lumen; RBC, red blood cell.

observations demonstrated elevated NET levels in children with active IgAV and in a rat model, which appeared to be associated with the severity of tissue injury (14,37). Mechanistically, aberrant glycosylation of IgA1 enhances its binding to FcαRI on neutrophils, promoting the shedding of soluble CD89 (sCD89) and the subsequent formation of pathogenic circulating sCD89-IgA complexes (4). Previous studies have indicated that IgA immune complexes, including sCD89-IgA complexes, may play a role in the development of IgAV (38). Genome-wide association studies further support a central role for the FcαRI pathway in IgAV susceptibility and pathogenesis (39). In IgAV-associated nephritis, circulating IgA1 complexes have been shown to induce FcαRI-dependent neutrophil activation, culminating in endothelial injury (40).

Because mice lack a direct ortholog of human FcαRI but express the related receptor Fcα/μR, which binds both IgA and IgM, we hypothesized that Fcα/μR might serve a compensatory role in NET induction during murine IgAV. Using a genetic knockout approach, the present study found that Fcα/μR deficiency markedly attenuated intestinal tissue injury and significantly suppressed NET formation in the IgAV model. Collectively, these findings suggest that Fcα/μR may act as a key upstream receptor in murine IgAV and may contribute to disease pathogenesis by promoting neutrophil activation and NET release.

The present findings further suggest that Fcα/μR may function as an upstream regulator of the pathogenic cascade in IgAV. In the WT model group, intestinal NET levels, quantified using the specific NET-associated complexes MPO-DNA and NE-DNA, were markedly elevated. This finding is consistent with the established role of NETs as potential drivers of vascular endothelial injury in other autoimmune and inflammatory vasculopathies (12,41-43). Notably, Fcamr-KO mice subjected to the same IgAV induction protocol did not exhibit a significant increase in NET formation, in marked contrast to their WT counterparts. Together, these results suggest that IgA immune complex-induced neutrophil activation and the subsequent release of pathogenic NETs may depend on Fcα/μR signaling in murine IgAV.

The present findings also support a possible mechanistic link between NET formation and intestinal inflammatory injury, potentially through activation of NLRP3 inflammasome-mediated pyroptosis. In WT model mice, marked upregulation was observed of intestinal proteins involved in inflammasome assembly (NLRP3 and ASC), the inflammasome effector protease cleaved caspase-1 and the pyroptosis executioner GSDMD-N, together with significantly elevated levels of the mature cytokines IL-1β and IL-18. TEM analysis further revealed characteristic pyroptotic ultrastructural changes in intestinal microvascular endothelial cells. Notably, genetic ablation of Fcamr not only reduced NET formation but also attenuated downstream events, including NLRP3 inflammasome activation, caspase-1 cleavage, GSDMD-N generation and IL-1β and IL-18 release. These coordinated changes suggest that NETs may trigger pyroptotic signaling in this setting and that the Fcα/μR-NET axis may serve as an upstream regulatory node. This interpretation is consistent with emerging evidence from other inflammatory conditions. Zhao *et al* (44) reported that NETs induced NLRP3-dependent pyroptosis in human pulmonary microvascular endothelial cells *in vitro* and that this effect was abolished by the NLRP3 inhibitor MCC950. They also observed pyroptotic features in pulmonary microvascular endothelial cells in a mouse model of interstitial lung disease. Similarly, Yu *et al* (45) reported that NETs contributed to intrahepatic coagulation, inflammation and fibrosis in mice subjected to bile duct ligation by inducing NLRP3 activation. The corresponding *in vitro* experiments suggested that NETs could induce liver sinusoidal endothelial cell dysfunction and activate NLRP3-mediated pyroptosis. Consistent with these findings, the present results in a mouse model of IgAV support the possibility that NETs induce pyroptosis in intestinal microvascular endothelial cells through activation of the NLRP3 inflammasome.

Beyond the central role of NLRP3, the coordinated activation of the canonical inflammasome complex was also examined in the present study. The concurrent upregulation of ASC, cleaved caspase-1 and GSDMD-N observed in the present model reflects the sequential assembly and activation of this complex. ASC functions as an essential adaptor linking NLRP3 to pro-caspase-1, and its oligomerization into speck-like structures represents a critical checkpoint in inflammasome activation (44,46). In pulmonary microvascular endothelial cells, stimulation with NETs increased the expression of ASC, NLRP3 and caspase-1, whereas these effects were attenuated by NET degradation or NLRP3 inhibition (44). Similarly, in bovine endometrial epithelial cells, NET stimulation upregulated ASC, NLRP3 and caspase-1, and these effects were reduced by DNase I-mediated NET degradation (46). Subsequent cleavage of pro-caspase-1 into its active form directly mediates GSDMD cleavage and the maturation of IL-1β and IL-18 (45,46). GSDMD-N then oligomerizes to form membrane pores, facilitating the release of IL-1β and IL-18 and ultimately leading to cell lysis (44-47). Although Zhao *et al* (44) reported elevated IL-1β levels in pulmonary endothelial cells, the authors did not assess IL-18. Yu *et al* (45) observed increased levels of both IL-18 and IL-1β in a hepatic model, consistent with caspase-1-dependent cytokine maturation. In the present study, the parallel increases in GSDMD-N, IL-1β and IL-18 in WT model mice, together with their concurrent reduction following Fcamr-KO, are consistent with activation of the complete NET-NLRP3-ASC-caspase-1-GSDMD-N-IL-1β/IL-18 axis during intestinal mucosal injury.

The functional relevance of this pathway is further supported by its involvement in intestinal inflammatory diseases. In dextran sulfate sodium-induced ulcerative colitis, GSDMD-mediated pyroptosis exacerbates mucosal injury, whereas inhibition of GSDMD cleavage or caspase-1 activity ameliorates disease severity (48). Similarly, blockade of the TXNIP-NLRP3-GSDMD signaling cascade in colonocytes attenuates pyroptosis and reduces colonic inflammation (49). Collectively, these findings implicate the NLRP3 inflammasome-GSDMD axis in intestinal mucosal injury. In the present IgAV model, reduced NET formation following Fcamr ablation was associated with attenuated pyroptosis and its downstream inflammatory consequences. However, whether this association reflects a direct causal relationship requires further investigation using targeted strategies to inhibit NET formation.

Notably, IL-18 levels were significantly elevated in the WT model group and reduced in the Fcamr-KO. Consistent with this observation, Shen *et al* (46) demonstrated upregulation of both IL-1β and IL-18 in NET-stimulated bovine endometrial epithelial cells. The parallel changes in these cytokines observed in our model are consistent with canonical inflammasome activation and suggest that IL-18 may contribute to intestinal inflammation, as previously implicated in acute lung injury (47). Future studies should directly determine whether specific NET components stimulate IL-18 release from intestinal endothelial cells to clarify this mechanism.

Several limitations of the present study should be acknowledged. First, direct *in vitro* evidence delineating the molecular mechanisms of Fcα/μR-mediated NETosis following IgA immune complex engagement is lacking. Second, although the present *in vivo* findings demonstrate a consistent association between NET and pyroptosis markers, direct evidence that NETs induce NLRP3 inflammasome-mediated endothelial pyroptosis remains unavailable. Future studies should use DNase I-mediated NET degradation in this murine model or stimulate endothelial cells *in vitro* with isolated NET components to establish causality (50-52). Third, mice lack human FcαRI and instead express Fcα/μR, which binds both IgA and IgM and has distinct affinity and signaling properties. Consequently, this murine model may not fully recapitulate FcαRI-mediated IgAV in humans. Extrapolation of these findings to the treatment of human IgAV should consequently be undertaken with caution and requires further validation in clinical studies or humanized models. These mechanistic questions warrant further investigation.

In summary, the present study suggests that Fcα/μR may function as a key upstream receptor promoting NET formation in a murine model of IgAV. The present findings are also consistent with the hypothesis that NETs may contribute to intestinal mucosal injury through activation of the NLRP3-ASC-caspase-1 inflammasome pathway and the associated induction of pyroptosis in microvascular endothelial cells. Collectively, these findings provide further insight into the pathogenesis of IgAV and highlight the potential involvement of the Fcα/μR-NET-pyroptosis axis in intestinal mucosal injury.

Acknowledgements

Not applicable.

Funding

The present study was supported by Guangxi Natural Science Foundation (grant no. 2024GXNSFAA010055), Middle/Young aged Teachers Research Ability Improvement Project of Guangxi Higher Education (grant no. 2024KY0093), Difficult and Critical Illness Center, Pediatric Clinical Medical Research Center of Guangxi (grant no. Gui Ke AD22035219), the Excellent Medical Talents Training Program of the First Affiliated Hospital of Guangxi Medical University, Guangxi College Students Innovative Entrepreneurial Training Plan Program (grant no. S202510598178).

Availability of data and materials

The data generated in the present study may be requested from the corresponding author.

Authors' contributions

FXQ performed the majority of the experiments, analyzed the data and drafted the initial manuscript. YLL conducted key validation experiments, participated in data interpretation and revised the manuscript. LH was responsible for the critical validation of the raw dataset, including outlier detection and integrity verification. QT participated in the interpretation of the validated data and edited the manuscript for language and clarity. LCL participated in animal model establishment, sample collection and manuscript revision. XY conceived the study, supervised the experimental work, and validated the findings. XQC led the study design, secured funding, and provided critical revisions to the manuscript. LH and QT confirm the authenticity of all the raw data. All authors read and approved the final version of the manuscript.

Ethics approval and consent to participate

All animal experiments were approved by the Guangxi Medical University Ethics Committee (approval no. 202406030).

Patient consent for publication

Not applicable.

Competing interests

The authors declare that they have no competing interests.

References

1. Piram M and Mahr A: Epidemiology of immunoglobulin A vasculitis (Henoch-Schönlein): Current state of knowledge. Curr Opin Rheumatol 25: 171-178, 2013.
2. Gardner-Medwin JM, Dolezalova P, Cummins C and Southwood TR: Incidence of Henoch-Schönlein purpura, Kawasaki disease, and rare vasculitides in children of different ethnic origins. Lancet 360: 1197-1202, 2002.
3. Nikolaishvili M, Pazhava A and Di Lernia V: Viral infections may be associated with Henoch-Schönlein purpura. J Clin Med 12: 697, 2023.
4. Pillebout E and Sunderkötter C: IgA vasculitis. Semin Immunopathol 43: 729-738, 2021.
5. Xu L, Li Y and Wu X: IgA vasculitis update: Epidemiology, pathogenesis, and biomarkers. Front Immunol 13: 921864, 2022.
6. Heineke MH, Ballering AV, Jamin A, Ben Mkaddem S, Monteiro RC and Van Egmond M: New insights in the pathogenesis of immunoglobulin A vasculitis (Henoch-Schönlein purpura). Autoimmun Rev 16: 1246-1253, 2017.
7. López-Mejías R, Genre F, Pérez BS, Castañeda S, Ortego-Centeno N, Llorca J, Ubilla B, Remuzgo-Martínez S, Mijares V, Pina T, *et al*: HLA-DRB1 association with Henoch-Schonlein purpura. Arthritis Rheumatol 67: 823-827, 2015.
8. Breedveld A and van Egmond M: IgA and FcalphaRI: Pathological roles and therapeutic opportunities. Front Immunol 10: 553, 2019.
9. Sugino H, Sawada Y and Nakamura M: IgA vasculitis: Etiology, treatment, biomarkers and epigenetic changes. Int J Mol Sci 22: 7538, 2021.

10. Mayer-Hain S, Gebhardt K, Neufeld M, Ehrchen JM, Molyneux K, Barratt J, Nattkemper E, Gerloff D, Roth J, Vogl T, *et al*: Systemic activation of neutrophils by immune complexes is critical to IgA vasculitis. J Immunol 209: 1048-1058, 2022.
11. Brinkmann V, Reichard U, Goosmann C, Fauler B, Uhlemann Y, Weiss DS, Weinrauch Y and Zychlinsky A: Neutrophil extracellular traps kill bacteria. Science 303: 1532-1535, 2004.
12. Papayannopoulos V: Neutrophil extracellular traps in immunity and disease. Nat Rev Immunol 18: 134-147, 2018.
13. Retter A, Singer M and Annane D: 'The NET effect': Neutrophil extracellular traps-a potential key component of the dysregulated host immune response in sepsis. Crit Care 29: 59, 2025.
14. Chen XQ, Tu L, Zou JS, Zhu SQ, Zhao YJ and Qin YH: The involvement of neutrophil extracellular traps in disease activity associated with IgA vasculitis. Front Immunol 12: 668974, 2021.
15. Chen XQ, Tu L, Tang Q, Zou JS, Yun X and Qin YH: DNase I targeted degradation of neutrophil extracellular traps to reduce the damage on IgAV rat. PLoS One 18: e0291592, 2023.
16. Liu Y, Pan R, Ouyang Y, Gu W, Xiao T, Yang H, Tang L, Wang H, Xiang B and Chen P: Pyroptosis in health and disease: Mechanisms, regulation and clinical perspective. Signal Transduct Target Ther 9: 245, 2024.
17. Shi J, Zhao Y, Wang K, Shi X, Wang Y, Huang H, Zhuang Y, Cai T, Wang F and Shao F: Cleavage of GSDMD by inflammatory caspases determines pyroptotic cell death. Nature 526: 660-665, 2015.
18. Bai Y, Pan Y and Liu X: Mechanistic insights into gasdermin-mediated pyroptosis. Nat Rev Mol Cell Biol 26: 501-521, 2025.
19. Swanson KV, Deng M and Ting JP: The NLRP3 inflammasome: Molecular activation and regulation to therapeutics. Nat Rev Immunol 19: 477-489, 2019.
20. Kelley N, Jeltema D, Duan Y and He Y: The NLRP3 inflammasome: An overview of mechanisms of activation and regulation. Int J Mol Sci 20: 3328, 2019.
21. Hou CC, Ma HF, Ye JF, Luo D, Bao HF and Guan JL: Plasma exosomes derived from patients with intestinal Behçet's syndrome induce intestinal epithelial cell pyroptosis. Clin Rheumatol 40: 4143-4155, 2021.
22. Han XY and Qi HR: Pyroptosis in Kawasaki disease: From mechanisms to targeted interventions. Front Immunol 16: 1566985, 2025.
23. Wei Z, An X, Xie Y, Shen Y, Ni L, Xu J, Wang Y, Shen P, Shi H, Zhang W and Chen Y: NLRP3 inflammasome activity and pyroptosis are involved in CD206 $^{+}$ macrophage activation by MPO anti-neutrophil cytoplasmic antibodies. Acta Biochim Biophys Sin (Shanghai) 57: 1791-1802, 2025.
24. Jia C, Zhang J, Chen H, Zhuge Y, Chen H, Qian F, Zhou K, Niu C, Wang F, Qiu H, *et al*: Endothelial cell pyroptosis plays an important role in Kawasaki disease via HMGB1/RAGE/cathespin B signaling pathway and NLRP3 inflammasome activation. Cell Death Dis 10: 778, 2019.
25. Kuo KC, Yang YL, Lo MH, Cai XY, Guo MM, Kuo HC and Huang YH: Increased expression of pyroptosis in leukocytes of patients with Kawasaki disease. Diagnostics (Basel) 11: 2035, 2021.
26. Hu Q, Shi H, Zeng T, Liu H, Su Y, Cheng X, Ye J, Yin Y, Liu M, Zheng H, *et al*: Increased neutrophil extracellular traps activate NLRP3 and inflammatory macrophages in adult-onset Still's disease. Arthritis Res Ther 21: 9, 2019.
27. Cui Y, Yang Y, Tao W, Peng W, Luo D, Zhao N, Li S, Qian K and Liu F: Neutrophil extracellular traps induce alveolar macrophage pyroptosis by regulating NLRP3 deubiquitination, aggravating the development of septic lung injury. J Inflamm Res 16: 861-877, 2023.
28. Jin J, Zhao Y, Fang Y, Pan Y, Wang P, Fan Z and Yu H: Neutrophil extracellular traps promote the activation of the NLRP3 inflammasome and PBMCs pyroptosis via the ROS-dependent signaling pathway in Kawasaki disease. Int Immunopharmacol 145: 113783, 2025.
29. van Gool MMJ and van Egmond M: IgA and FcαRI: Versatile players in homeostasis, infection, and autoimmunity. Immunotargets Ther 9: 351-372, 2021.
30. Shibuya A and Honda S: Immune regulation by Fcα/μ receptor (CD351) on marginal zone B cells and follicular dendritic cells. Immunol Rev 268: 288-295, 2015.
31. McDonald KJ, Cameron AJM, Allen JM and Jardine AG: Expression of Fc alpha/mu receptor by human mesangial cells: A candidate receptor for immune complex deposition in IgA nephropathy. Biochem Biophys Res Commun 290: 438-442, 2002.
32. Arifin WN and Zahiruddin WM: Sample size calculation in animal studies using resource equation approach. Malays J Med Sci 24: 101-105, 2017.
33. Tu Z, Guo H, Gao Y, Xiao W, Xie X, Yu H, Liang Q and Zhou Y: Macrophage pyroptosis mediates hyperoxia-induced inflammatory lung injury in neonates. Front Immunol 16: 1546986, 2025.
34. Ding R, Li H, Liu Y, Ou W, Zhang X, Chai H, Huang X, Yang W and Wang Q: Activating cGAS-STING axis contributes to neuroinflammation in CVST mouse model and induces inflammasome activation and microglia pyroptosis. J Neuroinflammation 19: 137, 2022.
35. Zhao Q, Dai MY, Huang RY, Duan JY, Zhang T, Bao WM, Zhang JY, Gui SQ, Xia SM, Dai CT, *et al*: Parabacteroides distasonis ameliorates hepatic fibrosis potentially via modulating intestinal bile acid metabolism and hepatocyte pyroptosis in male mice. Nat Commun 14: 1829, 2023.
36. Mann PC, Vahle J, Keenan CM, Baker JF, Bradley AE, Goodman DG, Harada T, Herbert R, Kaufmann W, Kellner R, *et al*: International harmonization of toxicologic pathology nomenclature: An overview and review of basic principles. Toxicol Pathol 40 (4 Suppl): 7S-13S, 2012.
37. Chen XQ, Zou JS, Tu L, Yun X and Qin YH: Neutrophil extracellular traps involved in the pathogenesis of IgA vasculitis: Confirmed in two IgAV rat models. PLoS One 18: e0288538, 2023.
38. Yu S, Zhang R, Lin Y, Lei K, Zhang J and Chang H: Blood soluble CD89-IgA complex may be a potential biomarker for predicting multi-organ involvement, especially renal involvement in children with immunoglobulin A vasculitis. Int Immunopharmacol 142: 113063, 2024.
39. Liu L, Zhu L, Monteiro-Martins S, Griffin A, Vlahos LJ, Fujita M, Berrouet C, Zanoni F, Marasa M, Zhang JY, *et al*: Genome-wide studies define new genetic mechanisms of IgA vasculitis. medRxiv [Preprint]: 2024.10.10.24315041, 2024.
40. Li Q, Wu H, Yuan X, Shi S, Liu L, Lv J, Zhang H and Zhu L: FcαRI-mediated neutrophil activation contributed to the pathogenesis of adult IgA vasculitis with nephritis. Nephrol Dial Transplant 41: 1274-1283, 2026.
41. Wu S, Chen Y, Jin X, Yu J, Chen X and Wan T: Toll like receptors promote high glucose-induced vascular endothelial cell dysfunction by regulating neutrophil extracellular traps formation. Inflammation 48: 3542-3559, 2025.
42. Zhang H, Wang Y, Qu M, Li W, Wu D, Cata JP and Miao C: Neutrophil, neutrophil extracellular traps and endothelial cell dysfunction in sepsis. Clin Transl Med 13: e1170, 2023.
43. Chu C, Wang X, Yang C, Chen F, Shi L, Xu W, Wang K, Liu B, Wang C, Sun D and Ding W: Neutrophil extracellular traps drive intestinal microvascular endothelial ferroptosis by impairing Fundc1-dependent mitophagy. Redox Biol 67: 102906, 2023.
44. Zhao P, Zhu J, Bai L, Ma W, Li F, Zhang C, Zhao L, Wang L and Zhang S: Neutrophil extracellular traps induce pyroptosis of pulmonary microvascular endothelial cells by activating the NLRP3 inflammasome. Clin Exp Immunol 217: 89-98, 2024.
45. Yu M, Zheng C, Li X, Ji X, Hu X, Wang X and Zhang J: Neutrophil extracellular traps-induced pyroptosis of liver sinusoidal endothelial cells exacerbates intrahepatic coagulation in cholestatic mice. Biochim Biophys Acta Mol Basis Dis 1871: 167700, 2025.
46. Shen W, Ma X, Shao D, Wu X, Wang S, Zheng J, Lv Y, Ding X, Ma B and Yan Z: Neutrophil extracellular traps mediate bovine endometrial epithelial cell pyroptosis in dairy cows with endometritis. Int J Mol Sci 23: 14013, 2022.
47. Liu C, Zhou Y, Tu Q, Yao L, Li J and Yang Z: Alpha-linolenic acid pretreatment alleviates NETs-induced alveolar macrophage pyroptosis by inhibiting pyrin inflammasome activation in a mouse model of sepsis-induced ALI/ARDS. Front Immunol 14: 1146612, 2023.
48. Ma ZR, Li ZL, Zhang N, Lu B, Li XW, Huang YH, Nouhoum D, Liu XS, Xiao KC, Cai LT, *et al*: Inhibition of GSDMD-mediated pyroptosis triggered by Trichinella spiralis intervention contributes to the alleviation of DSS-induced ulcerative colitis in mice. Parasit Vectors 16: 280, 2023.
49. Wang J, Zhang C, Qin J, An N, Bai M, Du RH, Shen Y, Wu XD, Cheng JC, Wu XF and Xu Q: Direct inhibition of the TXNIP-NLRP3-GSDMD pathway reduces pyroptosis in colonocytes and alleviates ulcerative colitis in mice by the small compound PEITC. Acta Pharmacol Sin 46: 2436-2449, 2025.

50. Cabral JE, Wu A, Zhou H, Pham MA, Lin S and McNulty R: Targeting the NLRP3 inflammasome for inflammatory disease therapy. Trends Pharmacol Sci 46: 503-519, 2025.
51. Coll RC, Hill JR, Day CJ, Zamoshnikova A, Boucher D, Massey NL, Chitty JL, Fraser JA, Jennings MP, Robertson AAB and Schroder K: MCC950 directly targets the NLRP3 ATP-hydrolysis motif for inflammasome inhibition. Nat Chem Biol 15: 556-559, 2019.
52. Zhang Y, Wu R, Zhan X, Wang XY, Xiang LW, Duan YQ, You Y, Zhang JB, Wu R, Zhang YY and Duan L: Neutrophil extracellular traps facilitate liver inflammation/fibrosis progression by entering macrophages and triggering AIM2 inflammasome-dependent pyroptosis. Cell Commun Signal 22: 556, 2024.

Copyright © 2026 Qin et al. This work is licensed under a Creative Commons Attribution-NonCommercial-NoDerivatives 4.0 International (CC BY-NC-ND 4.0) License.